DIRECT NUMERICAL SIMULATION OF TURBULENT FIBRE SUSPENSION SHEAR FLOW

Jurriaan J. J. Gillissen, Bendiks J. Boersma
Laboratory for Aero and Hydrodynamics, J.M. Burgers Center,
Technische Universiteit Delft
Leeghwaterstraat 21, 2628 CA Delft, The Netherlands
j.j.j.gillissen@wbmt.tudelft.nl

Geert Brethouwer
Department of Mechanics,
Kungliga Tekniska högskolan
SE-100 44 Stockholm, Sweden

Pål H. Mortensen, Helge I. Andersson
Department of Energy and Process Engineering,
Norwegian University of Science and Technology
7491 Trondheim, Norway

ABSTRACT

Turbulent channel and homogeneous shear flow of a suspension of non-Brownian elongated particles (fibres) are studied using Direct Numerical Simulation (DNS).

The effect of the fibres is governed by a stress tensor depending on the fourth order moments of the local distribution of fibre orientation, which is computed using the equation for the second moment of the distribution, involving a closure (Gillissen *et al.* 2007). The non-Newtonian fibre viscosity is defined as the ratio of dissipation due to fibre stress and Newtonian stress. It is demonstrated that the effect of the fibers can be modeled by adding the fibre viscosity to the molecular viscosity. In channel flow this yields nearly identical changes in flow structure as compared to the effect of the full constitutive equations.

Homogeneous shear flow of fibre suspension is compared to Newtonian shear flow. The effective viscosity (molecular plus fibre) is artificially kept equal in both flow. Similar evolution of the Reynolds stress anisotropy tensor, indicates that dynamics are the same. Fibre viscosity is shown to decrease and increase as a function of the shear number and Reynolds number, respectively. Within the ranges of Reynolds and shear numbers studied, the fibre viscosity is observed to depend on a single parameter. An analogy to rheology of Brownian fibres is drawn, in which turbulence is considered to induce diffusion on the distribution of fibre orientation.

INTRODUCTION

Suspended particles with a large length to diameter ratio $r \sim 10^3$ can induce significant changes in the turbulent structures of the carrier fluid at volume concentrations as low as $c \sim 10^{-5}$ (see for instance Paschkewitz *et al.* 2005). Most striking is the reduction of the drag coefficient in turbulent pipe flow. The mechanisms for drag reduction is a fundamental problem in fluid mechanics and numerical tools have widely been used to gain insight.

A distinction can be made between two types of elongated particles, rigid and flexible. Simulations have demonstrated that rigid particles (Paschkewitz *et al.* 2004) and flexible particles (Ptasinski *et al.* 2003) have very similar effects on turbulent boundary layer flow: reduced drag coefficient, increased energy and anisotropy in the velocity fluctuations, smaller strength and larger time and length scales of the near-wall vortical structures. Despite the fact that the dynamics of rigid particles (fibres) are substantially less complicated as compared to flexible particles, most research has addressed flexible particles and only a few numerical investigations on drag reduction in turbulent fibre suspension are reported.

In this paper we study turbulent channel and homogeneous shear flow of a suspension of non-Brownian fibres by means of Direct Numerical Simulation (DNS). We focus on the concept, of modeling the effect of the particles as an additional viscosity (Lumley 1969). Benzi *et al.* (2005) applied this idea in a one-equation turbulence model. They concluded that drag reduction originates from an additional viscosity which increases with wall-distance.

Our purpose is to explore the possibilities of modeling the effects of the fibres in a $k-\epsilon$ (two-equation) turbulence model (Wilcox 1993). Variables which need to be modeled are identified and measured using DNS. Empirical relations are constructed between these and the other $k-\epsilon$ variables.

GOVERNING EQUATIONS

Fibre suspension flow is governed by the incompressible Navier-Stokes equations, supplemented by the divergence of the fibre stress tensor $\boldsymbol{\tau}$ (Doi and Edwards 1986).

$$\rho\frac{D\boldsymbol{u}}{Dt} = \boldsymbol{\nabla}\cdot(-\Pi\boldsymbol{\delta} + 2\mu\boldsymbol{S} + \boldsymbol{\tau}) \qquad \boldsymbol{\nabla}\cdot\boldsymbol{u} = 0 \quad (1)$$

Here $D/Dt = \partial/\partial t + \boldsymbol{u}\cdot\boldsymbol{\nabla}$ is the material derivative, $\boldsymbol{\nabla}$ is the gradient operator, $\boldsymbol{\delta}$ is the unit tensor, $\boldsymbol{u}$ is the fluid velocity vector, Π is the pressure, ρ is the mass density and μ is the solvent dynamic viscosity.

The fibre stress $\boldsymbol{\tau}$ in Eq. (1) equals the rate of strain

$\boldsymbol{S} = \frac{1}{2}\left(\boldsymbol{\nabla u} + \boldsymbol{\nabla u}^T\right)$ projected on the fibre directional vectors by means of a double contraction with the fourth-order moment of the fibre distribution function as given by (Doi and Edwards 1986):

$$\boldsymbol{\tau} = 2\alpha\mu \boldsymbol{S} : \langle \boldsymbol{pppp} \rangle \qquad \alpha \sim cr^2/\ln r \tag{2}$$

Here $\boldsymbol{p}$ is the directional unit vector of an individual fibre, c is particle volume fraction and r is particle aspect-ratio. Eq. (2) involves averaging $\langle \cdots \rangle$ over fibres contained in a volume, surrounding the point at which the stress is to be determined. To compute $\boldsymbol{\tau}$ we use the equation for the second moment of the fibre distribution function.

$$\frac{D\langle \boldsymbol{pp} \rangle}{Dt} - \boldsymbol{\nabla u}^T \cdot \langle \boldsymbol{pp} \rangle - \langle \boldsymbol{pp} \rangle \cdot \boldsymbol{\nabla u} + 2\boldsymbol{\nabla u} : \langle \boldsymbol{pppp} \rangle = D\nabla^2 \langle \boldsymbol{pp} \rangle \tag{3}$$

The fourth-order moment $\langle \boldsymbol{pppp} \rangle$ is modeled using the closure developed by Wetzel who extended the method introduced by (Cintra and Tucker 1995). The right hand side of Eq. (3) models the effect of unresolved variations arising from turbulent advection at zero diffusivity (Batchelor 1959). Parameter D is referred to as artificial diffusivity. This approximate method was shown to provide very accurate results (Gillissen *et al.* 2007).

CHANNEL FLOW

Eqs. (1), (2) and (3) are integrated in the channel geometry, using the numerical method described in Gillissen *et al.* (2007). The flow is driven by means of a constant pressure gradient $-\partial\overline{\Pi}/\partial x$ between two parallel no-slip walls separated a distance H. The over-bar denotes Reynolds averaging (Tennekes and Lumley 1973). The Reynolds number $Re = U_\tau H/\nu = 360$ is based on the friction velocity $U_\tau = \sqrt{(1/2)(-\partial\overline{\Pi}/\partial x)(H/\rho)}$. Here $\nu = \mu/\rho$ is the kinematic solvent viscosity. The fibre concentration parameter $\alpha = 20$ and the artificial diffusivity $D = \nu$. The channel dimensions and resolutions in x (stream-wise), y (wall-normal) and z (span-wise) are $1.5H \times H \times 0.75H$ and $48 \times 192 \times 48$. According to Reynolds decomposition $\overline{\cdots}$, $(\cdots)'$ and $(\cdots)_{rms}$ denote mean part, fluctuating part and standard deviation. A variable with superscript $+$ is given in wall-units, i.e. it is scaled with μ, ρ and U_τ. Figs. 1a. and b compare first and second order fluid velocity statistics between the non-Newtonian fibre suspension flow and Newtonian flow ($\alpha = 0$). The increased mean velocity in the suspension as compared to Newtonian implies a reduced drag coefficient. Furthermore the energy and anisotropy in the velocity fluctuations increase, which is consistent with findings of previous research (Paschkewitz *et al.* 2004), (Ptasinski *et al.* 2003).

$K-\epsilon$ MODEL

The purpose of the present research is to make a first step towards a $k-\epsilon$ model (Wilcox 1993) of fibre suspension flow. The analysis presented here is restricted to the equations for mean momentum and turbulent kinetic energy $k = \overline{\boldsymbol{u'} \cdot \boldsymbol{u'}}/2$, whereas the equation for dissipation ϵ of turbulent kinetic energy will be studied in an upcoming work.

Mean momentum is governed by:

$$\left(\frac{\partial}{\partial t} + \overline{\boldsymbol{u}} \cdot \boldsymbol{\nabla}\right)\overline{\boldsymbol{u}} = \boldsymbol{\nabla} \cdot \left(-\overline{\boldsymbol{u'u'}} - \frac{\overline{\Pi}}{\rho}\boldsymbol{\delta} + 2\mu\overline{\boldsymbol{S}} + \frac{1}{\rho}\overline{\boldsymbol{\tau}}\right) \tag{4}$$

Within the $k-\epsilon$ model, the Reynolds stress is modeled as

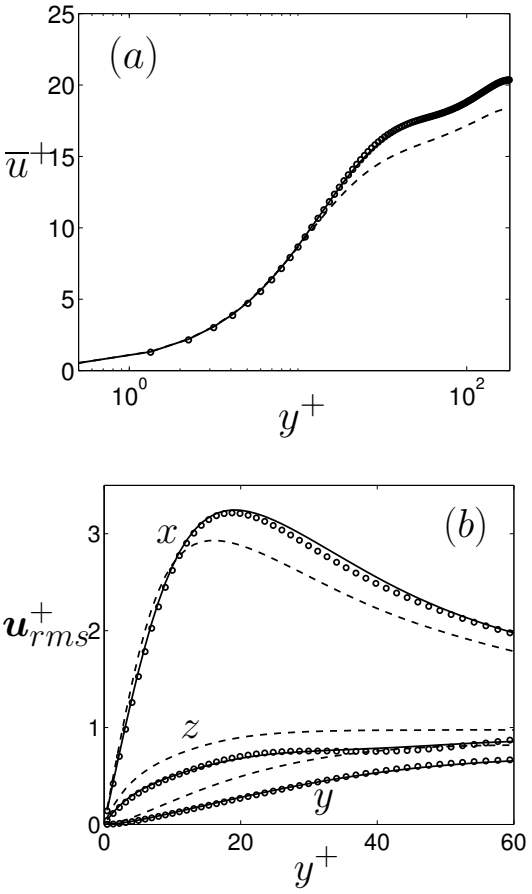

Figure 1: Mean (a) and standard deviation (b) of fluid velocity as a function of wall distance in channel flow. Comparison between Newtonian flow (dashed lines), fibre suspension flow computed with full constitutive equations (solid lines) and fibre suspension flow computed with (Eq. 7) (circles).

an eddy viscosity ν_T times the mean rate of strain tensor:

$$-\overline{\boldsymbol{u'u'}} = \nu_T \overline{\boldsymbol{S}} \qquad \nu_T = C_\mu \frac{k^2}{\epsilon} \tag{5}$$

with $C_\mu = 0.09$ a coefficient fitted to experimental data. In analogy to the modeling of the Reynolds stress, we pose for the mean fibre stress:

$$\frac{\overline{\boldsymbol{\tau}}}{\rho} = 2\alpha\nu\eta_M \overline{\boldsymbol{S}} \qquad \eta_M = \frac{1}{2\alpha\mu}\frac{\overline{\boldsymbol{S}} : \overline{\boldsymbol{\tau}}}{\overline{\boldsymbol{S}} : \overline{\boldsymbol{S}}} \tag{6}$$

The mean fibre viscosity η_M is formulated such that the dissipation of $\overline{\boldsymbol{u}} \cdot \overline{\boldsymbol{u}}$ due to fibre stress is modeled correctly. To investigate the validity of this approach we have simulated Eq. (1) in the channel geometry, where the fibre stress is modeled as:

$$\boldsymbol{\tau} = 2\alpha\mu\eta\boldsymbol{S} \tag{7}$$

in which the total fibre viscosity η is defined such that the dissipation resulting from Eq. (7) equals the dissipation predicted by the unmodeled constitutive equations (2) and (3):

$$\eta = \frac{1}{2\alpha\mu}\frac{\overline{\boldsymbol{S} : \boldsymbol{\tau}}}{\overline{\boldsymbol{S} : \boldsymbol{S}}} \tag{8}$$

In this simulation η was taken from the fibre suspension channel flow simulation, shown in Fig. 2a. In Figs. 1a

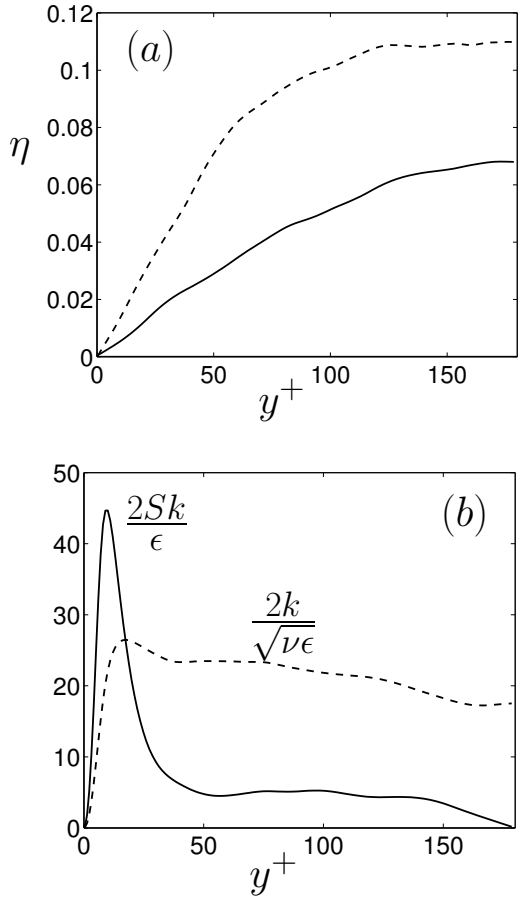

Figure 2: (a) Total fibre viscosity (Eq. 8) as a function of wall distance in channel flow. Non-Newtonian flow (solid line). Newtonian flow (dashed line). (b) Shear number and Reynolds number based on Taylor's micro-scale as a function of wall distance in Newtonian channel flow.

and b. simulation results are compared to those obtained using the full constitutive equations. Close correspondence indicates that the fibre stress is modeled well as an additional Reynolds averaged viscosity.

The equation of turbulent kinetic energy reads:

$$\left(\frac{\partial}{\partial t}+\overline{\boldsymbol{u}}\cdot\boldsymbol{\nabla}\right)k=-\overline{\boldsymbol{S}}:\overline{\boldsymbol{u'u'}}+$$
$$\boldsymbol{\nabla}\cdot\left[\overline{\left(-\left[\frac{\Pi'}{\rho}+k\right]\boldsymbol{\delta}+\frac{\boldsymbol{\tau'}}{\rho}\right)\cdot\boldsymbol{u'}}+\nu\boldsymbol{\nabla}k\right]-$$
$$\nu\left(2\overline{\boldsymbol{S'}:\boldsymbol{S'}}+\alpha\overline{\boldsymbol{S'}:\boldsymbol{\tau'}}\right) \qquad (9)$$

In the $k-\epsilon$ paradigm, the transport terms are modeled as $\boldsymbol{\nabla}\cdot\left(\overline{\boldsymbol{u'}\left[-\Pi'/\rho-k\right]}\right)=\boldsymbol{\nabla}\cdot(\nu_T/\sigma_k\boldsymbol{\nabla}k)$, where the coefficient $\sigma_k=1.0$ is based on experimental data. Although not dealt with here, it seems natural that the inclusion of $\boldsymbol{\nabla}\cdot\left(\overline{\boldsymbol{\tau'}/\rho\cdot\boldsymbol{u'}}\right)$ in the transport terms can be accounted for by a σ_k dependence on fibre properties. The dissipation due to fibre stress can be written as:

$$\nu\alpha\overline{\boldsymbol{S'}:\boldsymbol{\tau'}}=2\nu\alpha\eta_T\overline{\boldsymbol{S'}:\boldsymbol{S'}} \qquad \eta_T=\frac{1}{2\alpha\mu}\frac{\overline{\boldsymbol{S'}:\boldsymbol{\tau'}}}{\overline{\boldsymbol{S'}:\boldsymbol{S'}}} \qquad (10)$$

where η_T is referred to as the turbulent fibre viscosity.

Table 1: Parameters used in the homogeneous shear flow simulations. The markers correspond to the markers in Figs. 3-5.

RUN	S	$\frac{2Sk}{\epsilon}$ $(t=0)$	$\frac{2k}{\sqrt{\nu\epsilon}}$ $(t=0)$	α	Marker
1	2	3.3	15	0	▽
2	5	8.2	15	0	□
3	5	19	13	0	△
4	10	38	13	0	○
5	10	38	13	20	●

HOMOGENEOUS SHEAR FLOW

In order to construct a $k-\epsilon$ model of fibre suspension flow, relations are required for η_M and η_T. Our approach is to measure these variables in homogeneous shear flow by means of DNS, and relate them to other $k-\epsilon$ variables: k, ϵ, mean shear S and viscosity ν. We have chosen to study homogeneous shear flow, instead of channel flow, since DNS of channel flow is restricted to relatively low Reynolds numbers, which causes the near-wall region to dominate the flow. It is known that the $k-\epsilon$ model performs rather poor under these conditions.

In homogeneous shear flow the Reynolds averaged velocity is assumed $\overline{\boldsymbol{u}}=Sx_2\boldsymbol{\delta_1}$ with S the mean shear and $\boldsymbol{\delta_1}$ the unit vector in the stream-wise direction. Vector components in stream-wise, gradient-wise and span-wise directions are labeled 1, 2 and 3. In homogeneous shear, the equation of turbulent kinetic energy (Eq. 9) can be written as:

$$\frac{dk}{dt}=-S\overline{u_1'u_2'}-2\nu\left(1+\alpha\eta_T\right)\overline{\boldsymbol{S'}:\boldsymbol{S'}} \qquad (11)$$

where η_T is given in Eq. (10).

The fluctuations $\boldsymbol{u'}$ and the second moment of the fibre orientation distribution $\langle\boldsymbol{pp}\rangle$ are solved using an extended version of the computer code developed by Brethouwer (2005). Five runs are carried out: four Newtonian runs ($\alpha=0$) and one non-Newtonian run($\alpha=20$). The initial fields are generated from a simulation of decaying isotropic turbulence ($S=0$). The domain size and resolutions in x_1, x_2 and x_3 are $2\times1\times1$ and $256\times128\times128$. Relevant parameters are listed in table 1. In all simulations the effective viscosity

$$\nu_{eff}=\nu\left(1+\alpha\eta_T\right)=5\times10^{-3} \qquad (12)$$

To establish this in run 5, the molecular viscosity changes in time as $\nu=\nu_{eff}/\left(1+\alpha\eta_T\right)$. This is done to further explore the hypothesis that fibre stress can be modeled as additional viscosity. The artificial diffusion $D=\nu_{eff}$.

Runs 4 and 5 are compared in Fig. 3a, showing the time development of k and the dissipation $\epsilon=\nu_{eff}\overline{\boldsymbol{S'}:\boldsymbol{S'}}$ normalized with the values at $St=0$. It appears that energy and dissipation are smaller in the fibre suspension as compared to the pure solvent. Furthermore, the ratio ϵ/k is smaller in fibre suspension flow, indicating that the energy cascades at a smaller rate towards the dissipating scales. Despite these differences we argue that flow dynamics in Newtonian and fibre suspension shear flow are very similar when compared at constant ν_{eff}. The nearly identical time development of the Reynolds stress anisotropy tensor implies that the large scales have very similar structure in both flows (Fig. 3b). Therefore we conclude that fibre stress is modeled accurately as a viscous stress, when the fibre viscosity is chosen such that the resulting dissipation matches the unmodeled dissipation.

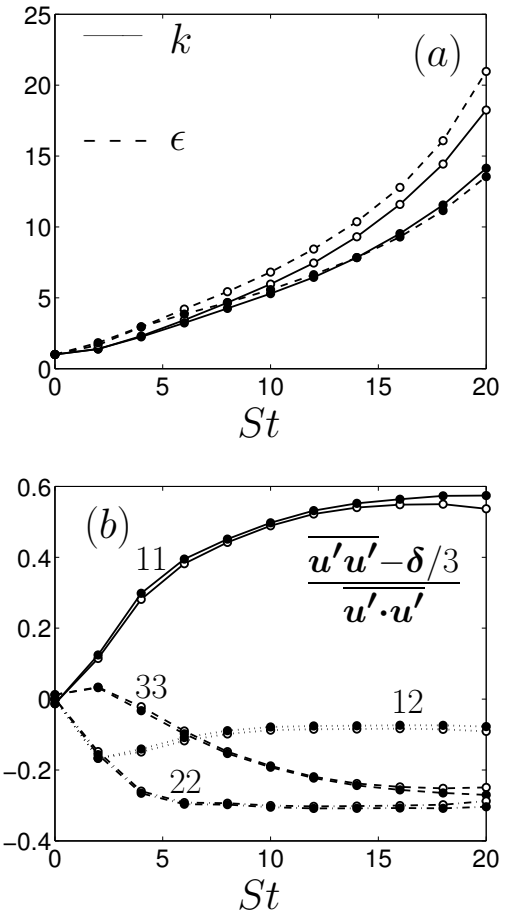

Figure 3: (a) Energy (solid lines) and dissipation (dashed lines), normalized by their initial values, as a function of time in homogeneous shear flow. Comparison between Newtonian flow (open circles) and fibre suspension flow (filled circles). (b) Components of the Reynolds anisotropy tensor as a function of time in homogeneous shear flow. Comparison between Newtonian flow (open circles) and fibre suspension flow (filled circles).

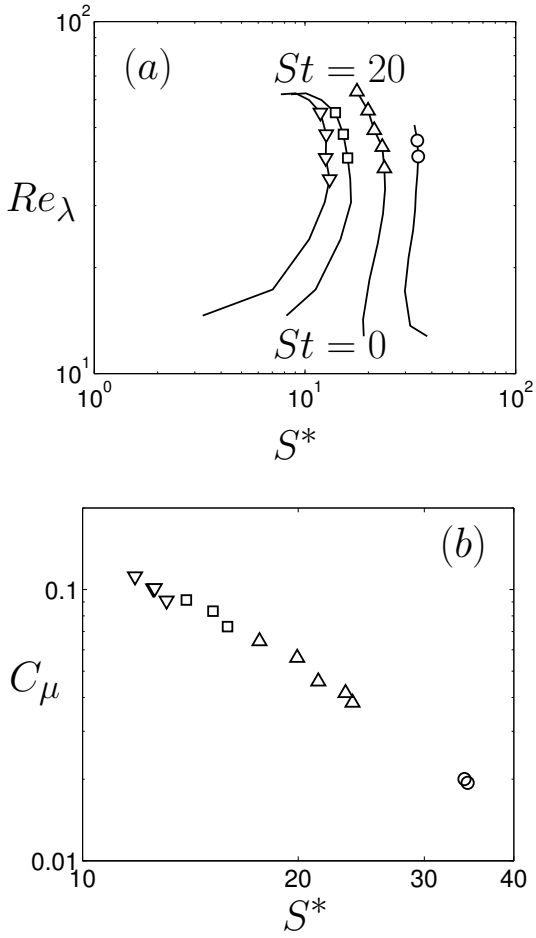

Figure 4: (a) Trajectories on the (shear number, Reynolds number)-plane for four simulations of Newtonian homogeneous shear flow. The markers indicate the different runs as described in table 1. (b) C_μ (Eq. 5) as a function of the shear number for four simulations of Newtonian homogeneous shear flow. The markers indicate the different runs as described in table 1.

In the following we focus on the Newtonian simulations, i.e. runs 1,2,3 and 4. The aim is to relate fibre viscosity to k, ϵ, S and ν, which could be used in a $k-\epsilon$ turbulence model. Based on these quantities, two independent dimensionless groups can be made. Here we use the shear number S^* and the Reynolds number based on Taylor's micro-scale Re_λ:

$$S^* = \frac{2Sk}{\epsilon} \qquad Re_\lambda = \frac{2k}{\sqrt{\nu\epsilon}} \tag{13}$$

The development of S^* and Re_λ for the four runs are shown in Fig. 4a. We focus on special time intervals. The interval starts when $t\epsilon/k \approx 1$. This is done, in order for the flow to have developed from isotropic to shear. The interval ends when the integral length scale of the velocity fluctuations (Tennekes and Lumley 1973) reaches half the domain-size. This is done, in order for the domain-size to have a negligible effect on the flow (Pumir 1996). The studied fields are indicated with the markers in Fig. 4a. Within these fields Re_λ varies between $40-65$ and S^* varies between $13-34$. For comparison we present the Reynolds number (0-25) and shear number (0-45) in channel flow in Fig. 2b.

Before turning to fibre viscosity, we first consider the relation for the eddy viscosity (Eq. 5). Fig. 4b shows that within the ranges of S^* and Re_λ considered, C_μ decreases one order of magnitude as a function of S^*, while being nearly independent of Re_λ. Since $k-\epsilon$ assumes constant C_μ this indicates one of its drawbacks.

A relation is sought between η_T (Eq. 10) and S^*, Re_λ. It is found that for the S^* and Re_λ ranges considered, a relation exist in terms of one parameter only: $S^* Re_\lambda^{\frac{-3}{4}}$. The exponent $\frac{-3}{4}$ is chosen such that the data taken from the four runs collapse on a single curve. This result is presented in Fig. 5a.

Similarly as for turbulent fibre viscosity, a relation is extracted for the mean fibre viscosity η_M (Eq. 6), which for shear flow reads:

$$\eta_M = \frac{1}{\alpha\mu}\frac{\overline{\tau_{12}}}{S} \tag{14}$$

For the parameter ranges considered, η_M is found to depend monotonically on $S^* Re_\lambda^{\frac{-1}{2}}$. To interpret this result an analogy is drawn to the rheology of a suspension of Brownian fibres. The fibre viscosity in laminar shear flow of such a

suspension:

$$\eta_B = \frac{1}{\alpha\mu}\frac{\tau_{12}}{S} \qquad \tau_{12} = \alpha\mu\left(2S\langle p_1p_1p_2p_2\rangle + 6d_B\langle p_1p_2\rangle\right) \tag{15}$$

is calculated from the Smulochowski equation (Doi and Edwards 1986):

$$S\boldsymbol{\nabla_p}\cdot(\boldsymbol{\delta_1\delta_2}\cdot\boldsymbol{p}\cdot(\boldsymbol{\delta}-\boldsymbol{pp})f) = d_B\nabla_{\boldsymbol{p}}^2 f \tag{16}$$

using the numerical method described in Gillissen *et al.* (2007). Here distribution function $f(\boldsymbol{p})$ gives the probability of finding a fibre with orientation $\boldsymbol{p}$, $\boldsymbol{\nabla_p}$ is the gradient operator on the unit sphere, and d_B is the Brownian rotary diffusivity $d_B = 3k_BT\log r/(\pi\mu L^3)$, with k_B the Boltzmann constant, T temperature and L fibre length. The averaging operator in Eq. (15) is related to f by: $\langle\cdots\rangle = \int\cdots f d\boldsymbol{p}$. Fig. 5b shows that η_B decreases as a function of S/d_B, known as shear-thinning (Doi and Edwards 1986). Matching the data for η_M to the shear thinning curve yields that the rotary diffusivity d_T induced by turbulence decreases with the fifth power of the shear number:

$$d_T \approx 0.25\frac{k}{\nu}S^{*-5}Re_\lambda \tag{17}$$

As can be seen from Fig. 5b, the analogy applies for $S/d_T > 10^2$. Furthermore, it must be noted that this result is based on a relatively small range of parameters. A wider parameter range will be studied in an up-coming work.

CONCLUSIONS

The effect of fibres on channel and homogeneous shear turbulence can be modeled as an additional Reynolds averaged viscosity. In channel flow this viscosity depends on wall distance, which causes changes in the near-wall vortical structures leading to drag reduction. In homogeneous shear turbulence this viscosity is homogeneous and non-Newtonian structures are nearly identical to Newtonian structures, when the flows are compared at the same effective viscosity (molecular plus fibre).

For the ranges of shear numbers and Reynolds numbers considered it is found that the fibre viscosity in homogeneous shear turbulence depends on a single dimensionless group, involving k, ϵ , S and ν. The findings of this research may serve as a guidance towards a formulation of a $k-\epsilon$ turbulence model of turbulent fibre suspension flow.

ACKNOWLEDGMENTS

The research has been partially supported through the PETROMAKS programme funded by The Research Council of Norway.

REFERENCES

Batchelor, G. K., 1959, "Small-scale variation of convected quantities like temperature in turbulent fluid. Part 1. General discussion and the case of small conductivity.", *J. Fluid Mech.* Vol. 5, pp. 113-133.

Benzi, R, Ching, E. S. C., Lo, T. S., L'vov, V. S. and Procaccia, I., 2005, "Additive equivalence in turbulent drag reduction by flexible and rod like Polymers.", *Phys. Rev. E* Vol. 72, pp. 016305.

Brethouwer, G., 2005, "The effect of rotation on rapidly sheared homogeneous turbulence and passive scalar transport. Linear theory and direct numerical simulation.", *J. Fluid Mech.*, Vol. 542, pp. 305-342.

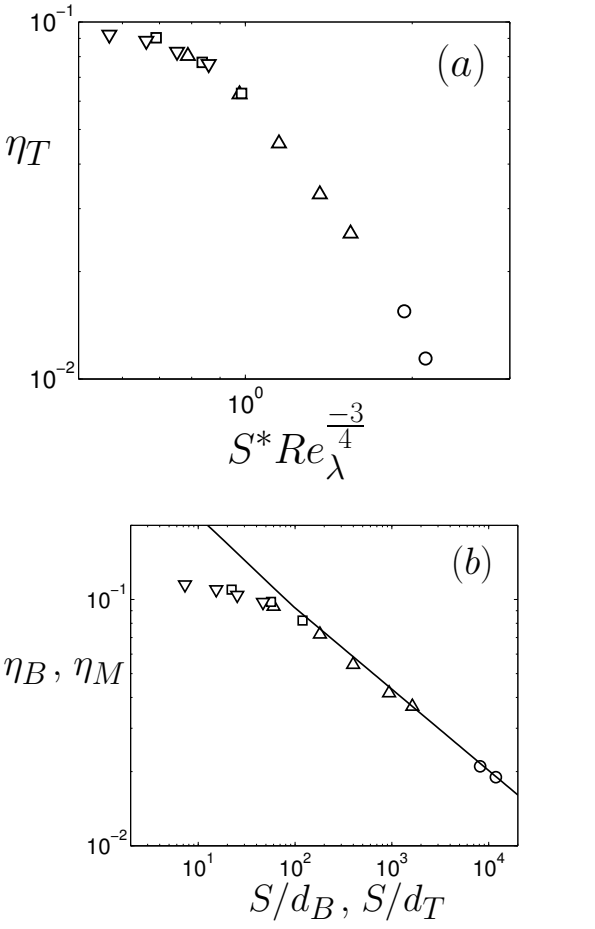

Figure 5: (a) Turbulent fibre viscosity in Newtonian homogeneous shear flow. Different markers correspond to the different runs, as described in table 1. (b) Line: Fibre viscosity η_B (Eq. 15) in simple shear for a suspension of Brownian fibres as a function of the shear rate, non-dimensionalized with the Brownian rotary diffusivity $d_B = 3k_BT\log r/(\pi\mu L^3)$. Markers: Mean fibre viscosity η_M (Eq. 14) in Newtonian homogeneous shear flow as a function of the mean shear rate, non-dimensionalized with the turbulent rotary diffusivity d_T (Eq. 17) Different markers correspond to the different runs, as described in table 1.

Cintra, J. S. and Tucker, C. L., 1995, "Orthotropic closure approximations for flow-induced fiber orientation.", *J. Rheol.* Vol. 39, pp. 1095-1122.

Doi, M.& Edwards S. F., 1986, "*The theory of polymer dynamics.*", Clarendon Oxford.

Gillissen, J. J. J. , Boersma, B. J. , Mortensen, P. H. ,Andersson, H. I., 2007, "On the performance of the moment approximation for the numerical computation of fibre stress in turbulent channel flow.", *Phys. Fluids* Vol. 19, pp 035102.

Lumley, J. L., 1969, "Drag reduction by additives.", *Ann. Rev. Fluid Mech.* Vol. 1, pp. 367-383.

Paschkewitz, J. S., Dubief, Y., Dimitropoulus, C. D., Shaqfeh, E. S. G. and Moin, P., 2004, "Numerical simulation of turbulent drag reduction using rigid fibres.", *J. Fluid Mech.* Vol. 518, pp. 281-317.

Paschkewitz, J. S., Dimitropoulus, C. D., Hou, Y. X., Somandepalli, V. S. R., Mungal, M. G., Shaqfeh, E. S. G. and

Moin, P., 2005, "An experimental and numerical investigation of drag reduction in a turbulent boundary layer using a rigid rodlike polymer.", *Phys. Fluids* Vol. 17, pp. 085101.

Ptasinski, P. K., Boersma B. J., Nieuwstadt, F. T. M., Hulsen, M. A., van den Brule, B. H. A., and Hunt, J. C. R., 2003, "Turbulent channel flow near maximum drag reduction: simulations, experiments and mechanisms.", *J. Fluid Mech.* Vol. 490, pp. 251-291.

Pumir, A. , 1996, "Turbulence in homogeneous shear flow.", *Phys. Fluids* Vol. 8, pp. 03112.

Tennekes, H., Lumley, J., L., 1973, "*A First Course in Turbulence.*", Cambridge: MIT Press.

Wilcox, D. C., 1993, "*Turbulence modeling for CFD.*", DCW Industries, La Canada, California.